International Journal of Minerals, Metallurgy and Materials
Volume 25, Number 1, January 2018, Page 53
https://doi.org/10.1007/s12613-018-1546-2

Effect of MWCNT reinforcement on the precipitation-hardening behavior of AA2219

Shijo Thomas and Umasankar V.

School of Mechanical and Building Sciences, VIT University, Chennai 600127, India
(Received: 11 April 2017; revised: 6 July 2017; accepted: 16 July 2017)

Abstract: Aluminum alloy matrix composites have found a predominant place in research, and their applications are explored in almost all industries. The aerospace industry has been using precipitation-hardenable alloys in structural applications. However, insufficient literature is available on the influence of multiwalled carbon nanotubes (MWCNTs) on precipitation-hardenable alloy composite materials; thus, this work was designed to elucidate the effect on MWCNT reinforcement on AA2219 with and without precipitation hardening. Reinforcement with MWCNTs has been reported to accelerate precipitation and to achieve greater hardness within a much shorter time. The addition of 0.75wt% MWCNTs resulted in maximal hardness at 90 min, which is approximately 27% of improvement over the maximum hardness achieved by the corresponding monolithic alloy after 10 h of aging. The sample reinforced with 0.75wt% MWCNTs showed an improvement of 82% in hardness by solutionizing and aging compared to that achieved by sintering.

Keywords: aluminum metal–matrix composites; multi walled carbon nanotubes (MWCNT); powder metallurgy; heat treatment; precipitation hardening

1. Introduction

Metal–matrix composites (MMCs) have been reported to demonstrate excellent toughness and ductility of the metal matrix and remarkable stiffness and strength with ceramic reinforcements. Because of their higher specific strength, MMCs have found applications in aerospace, military, automotive, and marine industries. Researchers in almost every industry are continuously exploring the possibilities for reducing weight without compromising other properties. The fact that the automotive industry is under pressure to improve fuel economy and reduce emissions while using materials with high specific strength and the ability to operate under high temperatures necessitates the development of suitable reinforcements to achieve these objectives. AA2219 alloy has been used in several space vehicles because of its weldability. Multiwalled carbon nanotubes (MWCNTs) have been garnering attention as a reinforcement material because of their unusual thermomechanical and electrical properties [1]. Because most AA2219 alloys undergo heat treatment and secondary processing before being used in structural applications, studies on the solutionizing and aging behavior of MWCNT-reinforced AA2219 composites and their effects on microstructure are appropriate. The mechanism of precipitation hardening and the effect of MWCNTs on precipitation hardening have received less attention among researchers [2]. Nam *et al*. [1], Meng *et al*. [2], and Choi *et al*. [3] have indicated the potential of MWCNTs in accelerating the precipitation rate during aging. "Precipitation hardening" or "age hardening" is a process by which strength and hardness of some metal alloys are improved via the formation of extremely small and homogeneously dispersed secondary-phase particles within the original phase matrix.

At higher volume fractions of MWCNTs, achieving a uniform distribution becomes a substantial challenge because MWCNTs tend to agglomerate rather than disperse. Semi-molten-state processing with a low pressure and a short sintering time is desirable for achieving good dispersion. Powder metallurgy achieves uniform dispersion of reinforcement particulates and improves the overall properties of MMCs. Spark plasma sintering (SPS) [4–9] provides rapid heating along with spark impact pressure and electrical field diffusion at the particle interface, which greatly en-

Corresponding author: Shijo Thomas E-mail: shijo.thomas3@gmail.com

hances the sintering rate with efficient densification. High heating and cooling rates with a short holding time will consolidate powder, without allowing sufficient time for agglomeration or grain growth [10].

2. Experimental methods

Gas-atomized pre-alloyed AA2219 powder (average particle size 42 μm) with high purity from AMPAL, USA and MWCNTs supplied by Redex India as per the specifications given in Table 1 were used in the present work. The chemical composition of the AA2219 alloy powder is listed in Table 2. Field-emission scanning electron micrographs of the AA2219 alloy powder and MWCNTs (as received) are shown in Fig. 1.

Table 1. MWCNT specifications

Purity	>97%
Bulk density	1.3 g/cm^3
Outer diameter	~20 nm
Inner diameter	~5 nm
Aspect ratio	~1000
Specific surface area	350 m^2/g

Table 2. Chemical composition of the AA2219 alloy powder

wt%

Al	Cu	Si	Mn	Fe	Zn	Ti	Zr
Balance	5.56	0.07	0.2	0.08	0.01	0.07	0.18

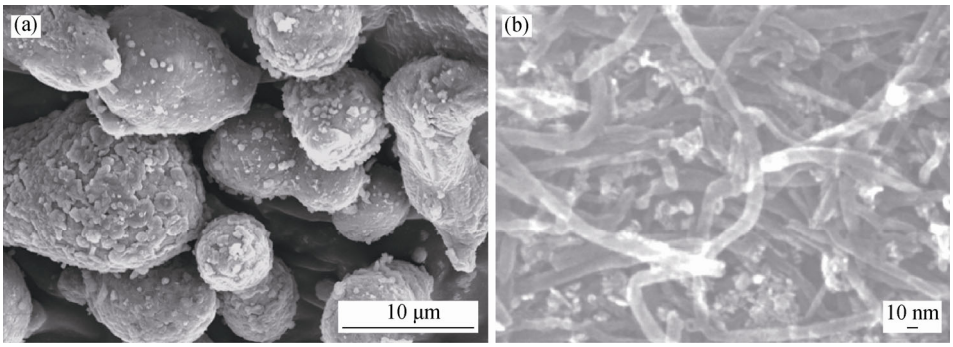

Fig. 1. Field-emission scanning electron microscopy (FESEM) images for (as received) AA2219 alloy powder (a) and MWCNTs (b).

The alloy powder was reinforced with 0.75wt% of MWCNTs. Agglomeration of CNTs can be reduced through the use of suitable mixing techniques. Solid diffusion because of the high impact energy of high-energy ball milling occurs during mechanical alloying of MWCNT–AA2219 powders [11–12]. Even though MWCNTs are embedded in the alloy matrix, the dispersion is not adequate. Sonication was effective in achieving a uniform dispersion of MWCNTs because it breaks down the clusters [13–14]. Effective dispersion was achieved by first dispersing MWCNTs in an ethanol solution via ultrasonication for 30 min; this process was repeated for next 1 h by adding alloy powder to the MWCNT solution, followed by wet ball milling (using methanol as the process control agent) in a laboratory planetary ball mill in a 250-mL cylindrical tungsten carbide jar with a ball-to-powder weight ratio (BPR) of 4:1 and at a speed of 250 r/min for 4 h. Sonication with subsequent ball milling can achieve better homogeneity than ball milling alone [13]. Fig. 2 shows a schematic of the synthesis of the AA2219–CNTs' metal matrix composite. A Dr. Sinter spark plasma sintering machine (SPS-625, SPS Syntex Inc., Japan) was used for powder consolidation. Premixed and ball-milled powders were filled into the graphite die and subjected to uniaxial pressing at 50 MPa and 500°C with a soaking time of 15 min. Here the heating rate was 100°C/min under vacuum and the heat source was pulsed DC; a sintered specimen of 20 mm in diameter and 10 mm in thickness was obtained. To prevent oxidation, the specimen was kept inside the vacuum chamber until the temperature was less than 70°C.

The sintered samples were subjected to a T6 heat treatment, as shown in Fig. 3. Spark-plasma-sintered samples were solutionized at 535°C for 70 min, as per American society for metals (ASM) recommendations [15]. Rapid cooling by quenching resulted in a supersaturated solid solution (SSSS) with trapped Cu atoms at room temperature. In the case of an AA2219 specimen with a 10-mm thickness, the quenching delay should not exceed 15 s and the quench should not exceed 37.7°C [15]. The solubility of Cu in Al at room temperature is only 0.1wt% [16]; the AA2219 alloy with 5.56wt% of Cu, upon rapid quenching after solutionizing, carries 55.6 times as much Cu as it is expected to carry at room temperature. This solubility variation induces precipitation. After solutionizing, artificial aging was carried out at 177°C for 10 h, as per ASM recommendations. In the present study, one set of samples was aged at 1.5 h to study the effect of MWCNTs on the acceleration of precipitation.

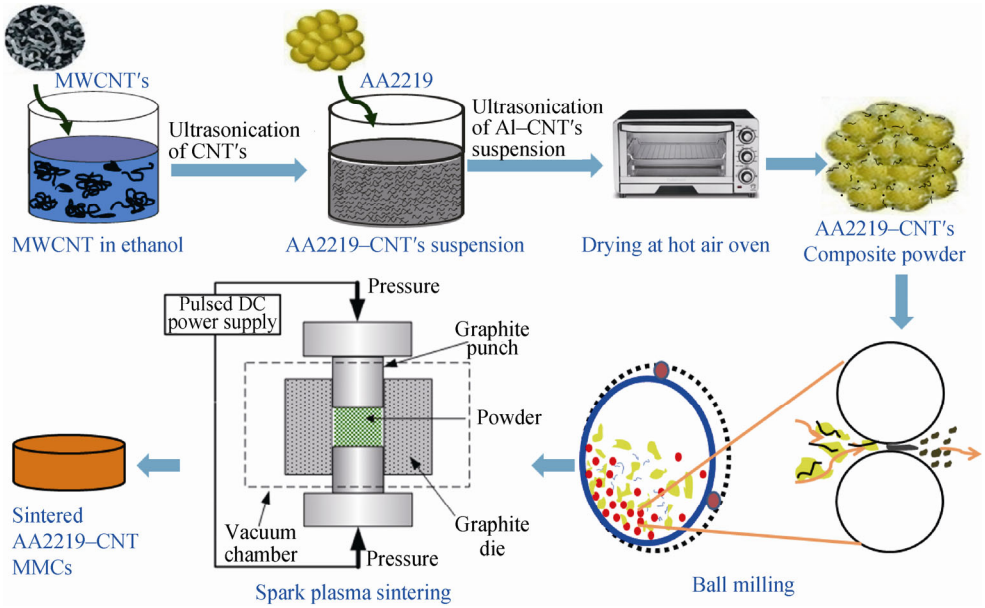

Fig. 2. Schematic representation of the synthesis of the AA2219–CNT nanocomposite.

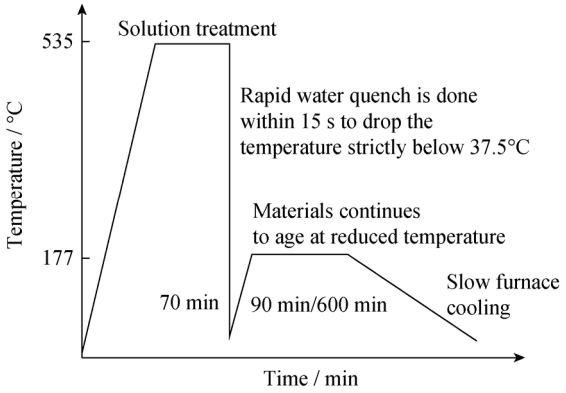

Fig. 3. T6 heat treatment and artificial aging for AA2219 and 0.75wt% MWCNT-reinforced composites.

The micrographs at each stage of solutionizing and aging were captured using optical microscopy (De-wintor inverted trinocular metallurgical microscope). Keller's reagent was used for etching sintered samples to resolve the grain boundary and the grains. Powder and bulk sample morphologies were characterized using scanning electron microscopy (SEM) (ZEISS EVO 18 Research) and FESEM (FESEM-SUPRA 55 - CARL ZEISS, Germany). The volume fraction of the precipitates was determined and analyzed with an elemental mapping system using energy-dispersive spectroscopy (EDS). FESEM micrographs show the MWCNT distribution in the AA2219 matrix after sintering, illustrating how the MWCNTs promote precipitation and result in improved hardness. X-ray diffraction (XRD) (Panalytical, The Netherland) was used for phase analysis. Mechanical properties were investigated using microhardness tests according to ASTM standard E384—16. The microhardness of the etched surface was measured by a Vickers microhardness tester (Shimadzu microhardness tester, HMV-G20) with test force $HV_{0.1}$ (980.7 mN) and a holding time of 15 s. Each composite was indented five times and the average value was reported.

3. Results and discussion

The relative density decreased from 99.71% to 94.84% with the addition of 0.75wt% MWCNTs because of the limited applied pressure during SPS [17]; however, excellent sinterability in a monolithic alloy gives good bonding with reduced porosity. The density of the Al–MWCNT samples might have been lower than the theoretical density because of the incoherency between the MWCNT particles and the Al matrix.

The microstructures of precipitation-hardening alloys change during heat treatment [18]. The etched matrix samples of AA2219 (Fig. 4(a)) retained the quantity of pores with clear fused boundaries. The effective fusion of grains at a uniform heating rate, a short soaking time, and a uniform thermal distribution reduced the number of pores. The effect of solution treatment close to the dissolution temperature of Cu in Al resulted in an SSSS. The alloy matrix after solutionizing at 535°C for 70 min (Fig. 4(b)) and aging (Figs. 4(c)–4(d)) did not show reduction or an increase in pores, as revealed by the pores not being affected even after sintering. Fig. 4(c) shows grain boundaries that are completely fused, without voids; it also shows primary alloy phase grains with precipitates. The increase in aging time to 10 h, where the structures are shown in Fig. 4(d), resulted in increased density of precipitates in each grain. Semi-coherent, disc-shaped, optical microscopically resolvable θ′ precipitates were obtained from coherent intermediate θ″ precipitates [18].

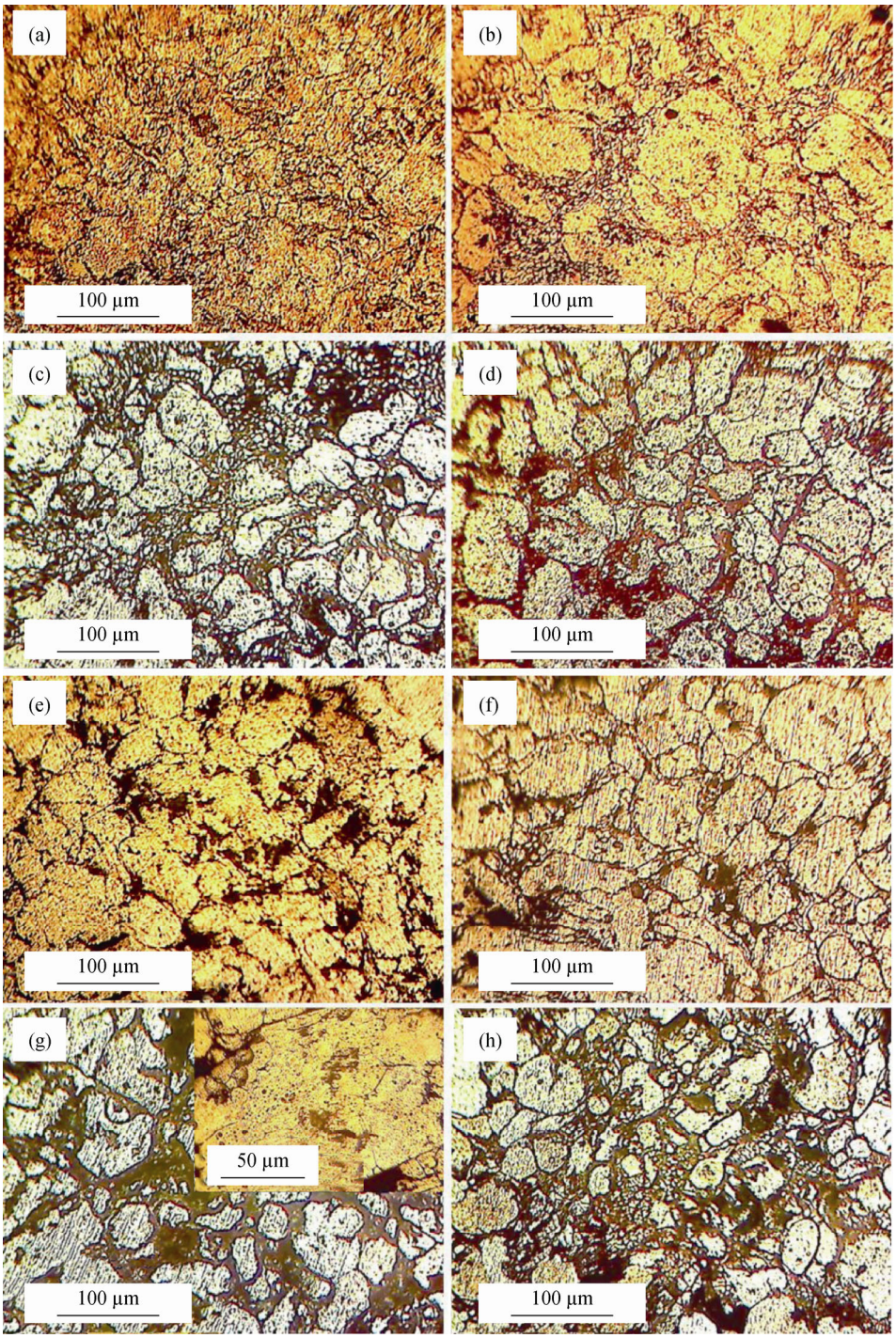

Fig. 4. Etched optical micrographs of AA2219 and AA2219 + 0.75wt% MWCNTs: (a,e) without heat treatment (as sintered); (b,f) after solution treatment; (c,g) after 90 min of aging; (d,h) after 10 h of aging.

From Figs. 4(a) and 4(e), the addition of CNTs resulted in the formation of more pores between the grains because of MWCNT clustering at grain boundaries (Fig. 5(b)). Pore formation decelerates the aging kinetics [17]. SPS processing can provide a better sinterability than conventional methods and can achieve improved peak hardness. Fig. 4(f) shows the reduction in porosity because of melting and fusion of the primary matrix. After solutionizing, very fine grains were formed between larger grains, which resulted in porosity reduction. A 90-min aging of AA2219 alloy with MWCNTs (Fig. 4(g)) increased the density of precipitates inside each grain with thick grain boundaries because of the accumulation of MWCNTs. A micrograph of the sample subjected to 10 h of aging (Fig. 4(h)) shows a

higher quantity of large $CuAl_2$ precipitates throughout the matrix. This result is an indication of over-aging. Finally, at low elastic strain, an incoherent θ ($CuAl_2$) equilibrium precipitate will form [18], which will soften the alloy. High-temperature aging and over aging cause easy formation of θ precipitates [18]. MWCNTs accelerate the aging kinetics; thus, θ precipitates will form within a short aging time.

FESEM micrographs of SPS-processed AA2219 reinforced with MWCNTs are shown in Fig. 5. Fig. 5(a) shows $CuAl_2$ as bright particles scattered over the surface, and Fig. 5(b) shows some MWCNT clustered in grain boundaries of the sintered samples. The density difference between reinforced CNTs and the AA2219 matrix and the large size difference of the aluminum alloy powder will hinder the distribution of MWCNTs. During solutionizing, the scattered $CuAl_2$ particles aggregated around the grain boundaries, along with Al_2O_3 (Fig. 5(c)). More oxidation is also observed in these regions. Similar effects are observed in sintered monolithic alloys. In the grain boundaries of

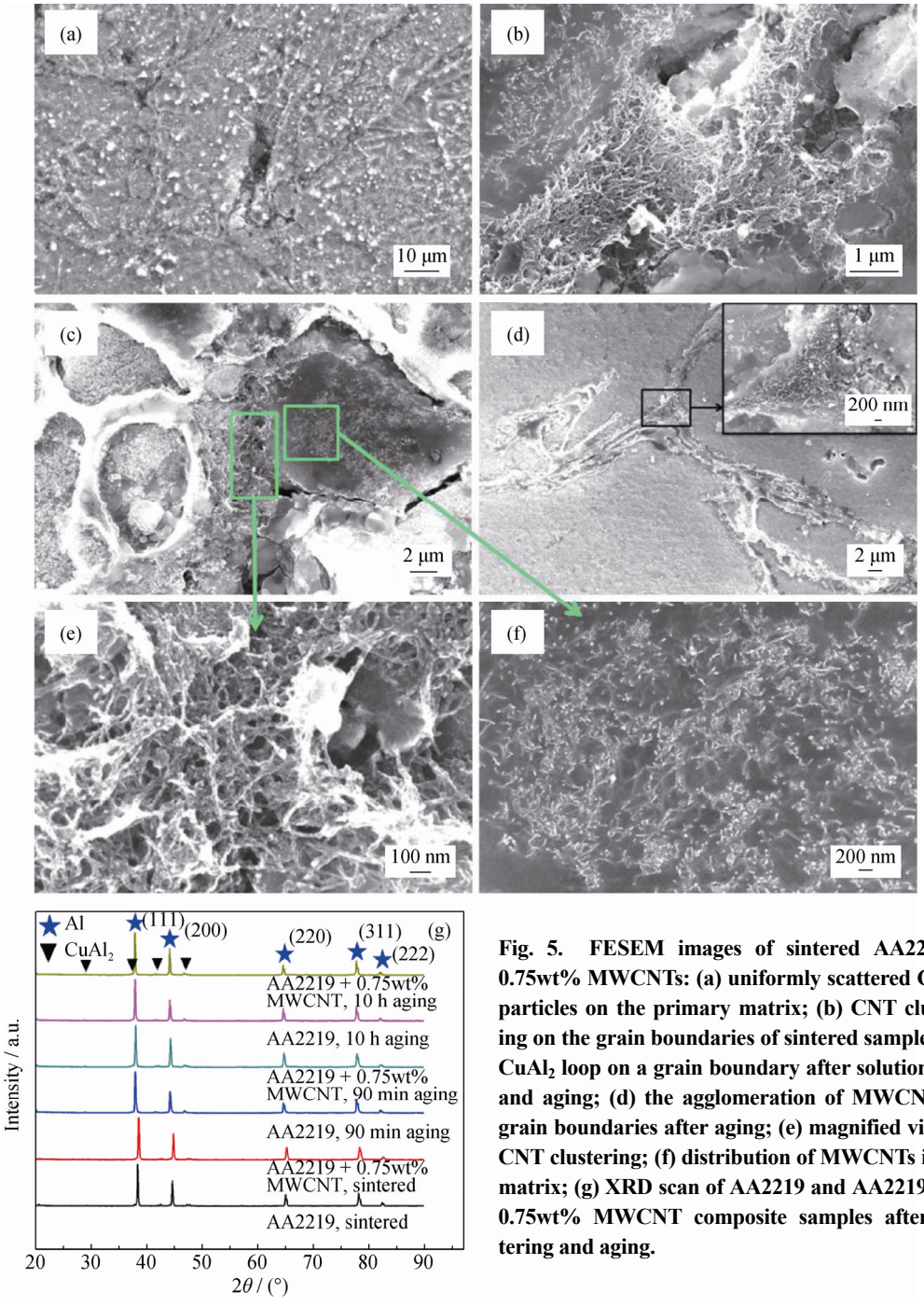

Fig. 5. FESEM images of sintered AA2219 + 0.75wt% MWCNTs: (a) uniformly scattered $CuAl_2$ particles on the primary matrix; (b) CNT clustering on the grain boundaries of sintered samples; (c) $CuAl_2$ loop on a grain boundary after solutionizing and aging; (d) the agglomeration of MWCNTs at grain boundaries after aging; (e) magnified view of CNT clustering; (f) distribution of MWCNTs in the matrix; (g) XRD scan of AA2219 and AA2219 with 0.75wt% MWCNT composite samples after sintering and aging.

MWCNT-reinforced samples, MWCNT clustering is observed (Figs. 5(b)–5(e)). However, the MWCNTs were uniformly distributed within the grains (Fig. 5(f)).

Solutionizing followed by aging did not induce any drastic changes in the position of MWCNTs; thus, the MWCNTs can hinder the grain growth during heat treatment. Accelerated nucleation and growth of precipitates were observed when the grain size was reduced because fine grains can enhance the aging kinetics [17]. The solutionizing and aging sample showed a maximum hardness along grain boundaries throughout the samples. The presence of $CuAl_2$ and MWCNTs in grain boundaries contributed to the maximum hardness across the grain boundaries after aging.

The MWCNT-bearing AA2219 sample subjected to SPS processing exhibits a diffraction pattern similar to that of the pure AA2219 under SPS, even after the addition of 0.75wt% of MWCNTs. The XRD scan did not show any clear evidence of carbide phase formation under SPS conditions and solutionizing followed by aging. A possible reason for the lack of carbide formation is that the MWCNTs are well dispersed in the matrix without inducing any structural damage and the amount of MWCNTs used was small. The XRD results show that the Cu elemental phase is converted into the $CuAl_2$ phase during the procedure of sintering. We observed that the $CuAl_2$ peak intensity in the XRD patters of both reinforced and unreinforced samples was improved after aging. The peak observed at 38.6° corresponds to the (111) planes of sintered AA2219 and sintered AA2219 + 0.75wt% MWCNT samples. The peaks were shifted to 37.9° after solutionizing followed by 90 min and 10 h of aging. Similarly, in the case of sintered monolithic and reinforced samples, observed peaks at 44.7°, 65.1°, and 78.4°, which correspond to the (200), (220), and (311) planes, respectively, shifted to 44.2°, 64.6°, and 77.8° after aging.

Precipitation of Cu atoms depends on the initial Cu concentration and the aging temperature [18]. Figs. 6(a)–6(f) show the SEM images of AA2219 specimens subjected to different heat-treatment conditions and the corresponding Cu mapping images. Figs. 7(a)–7(f) show the SEM images of the AA2219 with 0.75wt% MWCNT samples treated

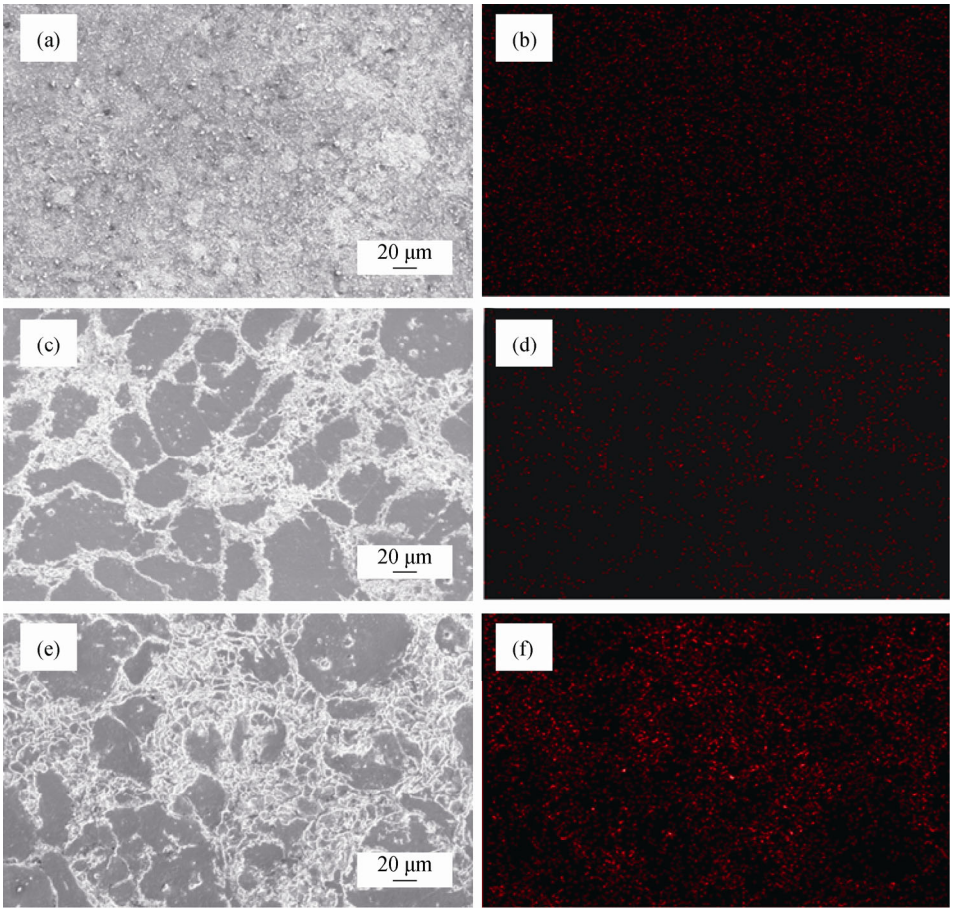

Fig. 6. SEM images of AA2219 and corresponding Cu mapping images: (a,b) without heat treatment (as sintered); (c,d) after 90 min of aging; (e,f) after 10 h of aging.

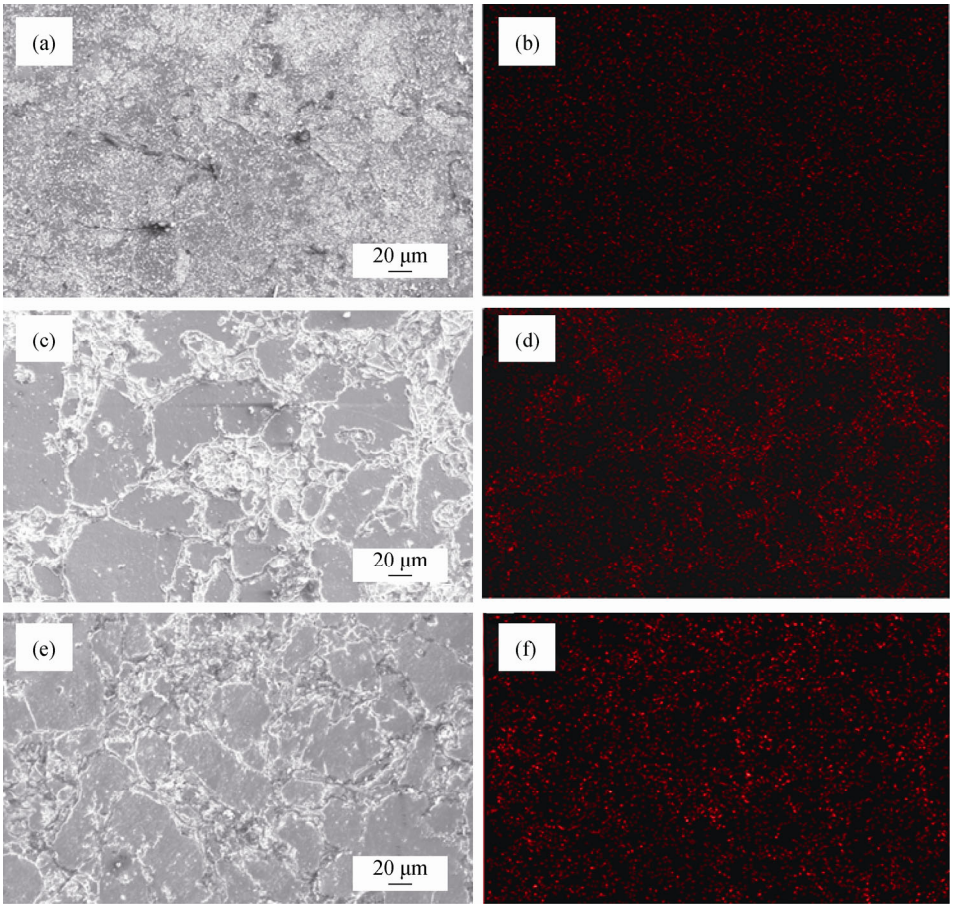

Fig. 7. SEM images of AA2219 + 0.75wt% MWCNTs and the corresponding Cu mapping images: (a,b) without heat treatment (as sintered); (c,d) after 90 min of aging; (e,f) after 10 h of aging.

under different conditions and the corresponding Cu mapping images. The Cu EDS mapping images for the sintered sample show the uniformly distributed $CuAl_2$ on grains after sintering. After solutionizing, a drastic change was observed in grain boundaries by the accumulation of $CuAl_2$ along the grain boundaries. The coefficient of thermal expansion for carbon nanotubes is lower than that of commercial pure aluminum [19]. Solutionizing causes matrix particles to expand and MWCNTs to contract because of thermal mismatch. It also causes the formation of microscopic gaps between MWCNT clusters as a result of the reduction in bonding between the matrix and the CNTs [17]. This reduced bonding results in reduced hardness of the composite after sintering and solutionizing; at the same time, it will accelerate aging by giving a pathway for precipitates. EDS mapping of solutionizing followed by aging indicates the presence of Cu along the grain boundaries as well as in primary α grains. Peak hardness was observed at the coherent intermediate θ″ precipitate zone due to increased density of coherent precipitates [18]. The MWCNT-reinforced 2219 alloy exhibits improved intensity of Cu in the EDS mapping images, which indicates a substantial improvement in hardness of approximately 34% compared with the hardness of the monolithic alloy after 90 min of aging. The EDS map of the 10-h-aged monolithic alloy shows an improvement in intensity of precipitates, whereas the reinforced sample shows the retardation of intensity of fine θ precipitates. Maximum hardness would occur at fine precipitates with retention of the crystalline characteristics of the θ phase [20]. If the distance between the precipitates is larger (low intensity), rejoining of dislocations will occur through extension of dislocations in the gap between precipitates, resulting in further dislocation motions [20]. As a result of 10-h aging, the monolithic alloy exhibited improved hardness; however, the reinforced sample exhibited a reduction in hardness from its peak hardness value because of over-aging. During over-aging, the intermediate phase began to form, causing recrystallization, softening, and a decrease in strength. The hardness value (Fig. 8) varies with respect to the changes in EDS mapping.

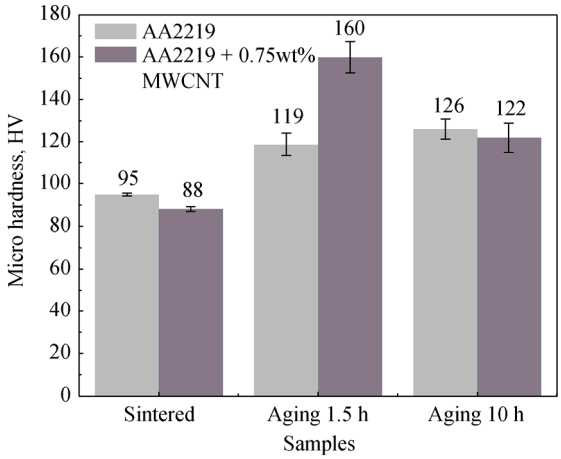

Fig. 8. Hardness variations for reinforced and unreinforced AA2219 (as sintered) and after aging.

Increased bonding resulted in better hardness in the monolithic alloy, whereas MWCNT agglomeration at grain boundaries reduced the hardness of reinforced samples. Solutionizing followed by 90 min of aging of the monolithic resulted in 25% of improvement in hardness, whereas the 0.75wt% MWCNT-reinforced samples achieved a substantial improvement of 82% in peak hardness. Nano sized precipitates might have formed coherent or semi-coherent interface structures with the matrix, resulting in a substantial increase of hardness. The AA2219 alloy achieved 33% improvement in hardness and the reinforced samples showed retardation in hardness after 10 h of aging. Similar effects were observed for conventionally sintered AA2219 with 0.75wt% MWCNT. The CNT-reinforced samples sintered by SPS and conventional methods show retardation in hardness after 10 h of aging.

4. Conclusions

The microstructural and mechanical behavior of aluminum alloy AA2219 composites reinforced with MWCNTs fabricated by the SPS process were observed and investigated; the effects of MWCNT reinforcement on the precipitation-hardening behavior of AA2219 aluminum alloy were investigated using FESEM, SEM-EDS, XRD, and a Vickers microhardness tester. Following conclusions can be obtained.

(1) Reinforcing with MWCNTs provides a dual advantage of improved hardness compared with that of the monolithic alloy and the additional benefit of achieving peak hardness within a very short aging time.

(2) With a short aging period of 90 min, AA2219 with 0.75wt% MWCNTs exhibited a noticeable improvement of 82% in hardness. By comparison, the unreinforced alloy achieved an improvement of 33% in peak hardness at 10 h of aging.

(3) The MWCNT-reinforced sample exhibited 27% improvement in hardness compared to the unreinforced sample after the T6 heat treatment. This result means that MWCNT addition accelerated the age-hardening kinetics of AA2219 alloys because of the increased dislocation density as a consequence of the coefficient of thermal expansion mismatch between the matrix and the CNTs during solutionizing. Also, grain boundaries and MWCNTs provide a pathway for Cu diffusion, stimulating the precipitate formation.

References

[1] D.H. Nam, Y.K. Kim, S.I. Cha, and S.H. Hong, Effect of CNTs on precipitation hardening behavior of CNT/Al–Cu composites, *Carbon*, 50(2012), No. 13, p. 4809.

[2] X. Meng, T. Liu, C.S. Shi, E.Z. Liu, C.N. He, and N.Q. Zhao, Synergistic effect of CNTs reinforcement and precipitation hardening in in-situ CNTs/Al–Cu composites, *Mater. Sci. Eng. A*, 633(2015), p. 103.

[3] H.J. Choi, B.H. Min, J.H. Shin, and D.H. Bae, Strengthening in nano structured 2024 aluminum alloy and its composites containing carbon nanotubes, *Composites Part A*, 42(2011), No. 10, p. 1438.

[4] N. Saheb, Sintering behavior of CNT reinforced Al6061 and Al2124 Nanocomposites, *Adv. Mater. Sci. Eng.*, 2014(2014), p. 1.

[5] A. Khalil, A.S. Hakeemand, and N. Saheb, Optimization of process parameters in spark plasma sintering Al6061and Al2124 aluminum alloys, *Adv. Mater. Res.*, 328-330(2011), p.1517.

[6] N. Saheb, Z. Iqbal, A. Khalil, A.S. Hakeem, N.A. Aqeeli, T. Laoui, A. Al-Qutub, and R. Kirchner, Spark plasma sintering of metals and metal matrix nanocomposites: a review, *J. Nanomater.*, 2012(2012), art. No. 18.

[7] Z.F. Liu, Z.H. Zhang, J.F. Lu, A.V. Korznikov, E. Korznikova, and F.C. Wang, Effect of sintering temperature on microstructures and mechanical properties of spark plasma sintered nanocrystalline aluminum, *Mater. Des.*, 64(2014), p. 625.

[8] G.A. Sweet, M. Brochu, R.L. Hexemer Jr., I.W. Donaldson, and D.P. Bishop, Microstructure and mechanical properties of air atomized aluminum powder consolidated via spark plasma sintering, *Mater. Sci. Eng. A*, 608(2014), p. 273.

[9] S. Rudinsky, J.M. Aguirre, G. Sweet, J. Milligan, D.P. Bishop, and M. Brochu, Spark plasma sintering of an Al-based powder blend, *Mater. Sci. Eng. A*, 621(2015), p. 18.

[10] S.R. Bakshi, D. Lahiri, and A. Agarwal, Carbon nanotubes reinforced metal matrix composites — a review, *Int. Mater. Rev.*, 55(2010), No. 1, p. 41.

[11] B. Chen, K. Kondoh, H. Imai, and J. Umeda, Effect of initial state on dispersion evolution of carbon nanotubes in alumi-

nium matrix composites during a high-energy ball milling process, *Powder Metall.*, 59(2016), No. 3, p. 216.

[12] J.Z. Liao and M.J. Tan, Mixing of carbon nanotubes (CNTs) and aluminum powder for powder metallurgy use, *Powder Technol.*, 208(2011), No. 1, p. 42.

[13] A.M.K. Esawi, K. Morsi, A. Sayed, M. Taher, and S. Lanka, Effect of carbon nanotube (CNT) content on the mechanical properties of CNT-reinforced aluminium composites, *Compos. Sci. Technol.*, 70(2010), No. 16, p. 2237.

[14] V. Giridhar, R.S. Arunraj, and R. Dhisondhar, Ultrasonic nano-dispersion technique of aluminium alloy and carbon nano-tubes (CNT) for automotive parts applications, *Int. J. Eng. Tech. Res.*, 1(2013), No. 7, p. 54.

[15] American Society for Metals, *Metals Handbook. Vol. 2: Heat Treating Cleaning and Finishing*, ASTM International, 1964.

[16] M.H. Jacobs, *TALAT Lecture: Precipitation hardening*, European Aluminium Association, Brussels, 1999, p. 1.

[17] N. Saheb, A. Khalil, A.S. Hakeem, T. Laoui, N. Al-Aqeeli, and A.M. Al-Qutub, Age hardening behavior of carbon nanotube reinforced aluminum nanocomposites, *J. Nano Res.*, 21(2013), p. 29.

[18] V.M.J. Sharma, K. Sree Kumar, B. Nageswara Rao, and S.D. Pathak, Studies on the work hardening behavior of AA2219 under different aging treatments, *Metall. Mater. Trans. A*, 40(2009), p. 3186.

[19] A. Agarwal, S.R. Bakshi, and D. Lahiri, *Carbon Nanotubes: Reinforced Metal Matrix Composites*, CRC Press of Taylor & Francis Group, 2010, p. 325.

[20] I.J. Polmear, Aluminium alloys — a century of age hardening, *Mater. Forum*, 28(2004), p. 1.